PERGAMON

International Journal of Heat and Mass Transfer 44 (2001) 2345–2356

International Journal of HEAT and MASS TRANSFER

www.elsevier.com/locate/ijhmt

Transient cooling of a two-phase medium of spherical shape when exposed to the rarefied cold environment

Seung Wook Baek [a,*], Jae Hyun Park [a], Shin Jae Kang [b]

[a] *Division of Aerospace Engineering, Department of Mechanical Engineering, Korea Advanced Institute of Science and Technology, 373-1 Kusung-dong, Yusung-ku, Taejon 305-701, South Korea*

[b] *Department of Mechanical Engineering, Chonbuk National University, Dukjin-ku, Chonju 561-756, South Korea*

Received 6 September 1999; received in revised form 1 May 2000

Abstract

Unsteady cooling problem with conduction and two-phase radiation are numerically analyzed here for a spherical two-phase (gas–particle) medium exposed to the rarefied cold environment. Two-phase radiative transfer equation (RTE) affected by both gas and particle phases is taken into consideration. This nonlinear integro-differential RTE is solved by using the discrete ordinates method (DOM, or the so-called S_N method). A parametric study is performed by changing the conduction-to-radiation parameter, optical thickness, convection-to-radiation parameter, gas and particle absorption-to-extinction ratio, wall emissivity and heat capacity ratio. Thermal characteristics are discussed through spatial temperature distribution, transient mean temperature variation, and radiative heat loss. The results confirm the significant effects of the two-phase radiation on the unsteady thermal characteristics for two-phase medium.

1. Introduction

A combined conductive and radiative heat transfer problem in a spherical geometry has been constantly attractive to many researchers. However, most previous works have dealt with a single-phase medium [1,2], while much less attention has been paid to two-phase mixture with gas and particles. Since the particle suspended gas has a higher heat capacity than gas only and no phase change occurs in the flow, the two-phase mixture is expected to be used for enhancing heat transfer in engineering applications [3,4]. Typical application lies in cooling of high temperature porous ceramic insulating media and waste heat dissipation technique for an orbiting space power plant [5,6].

In order to understand the combined heat transfer in two-phase medium, it is essential to rigorously treat the radiation exercised by gas and particles together. Nevertheless, only a limited number of works regarding two-phase radiation are available whereas many studies have been performed for single-phase radiation in the past decades. Previously, when treating the two-phase radiation, the absorption and emission by one of two phases have been neglected. That is to say, it is usually assumed that only the gas participates in absorption and emission while particles in scattering, or only the particles are involved in absorption, emission, and scattering while the gas is transparent to the radiation. However, this approach is not complete in the sense of dealing with the two-phase radiation so that some error is incurred in predicting the radiation effect [7]. Consequently, different from the previous studies, complete radiation by gas and particles are taken into account in this study. It is done by deriving the radiative transfer equation (RTE) considering the thermal nonequilibrium between gas and particles and by introducing the separate divergence of radiative heat flux by gas and particles into respective energy equation for gas and particles [7].

In this study, the two-phase radiation is examined in the problem of a transient cooling of a gas–particle two-phase medium in spherical shape, when it is exposed to the rarefied blackbody environment. Inside the medium,

* Corresponding author. Tel.: +82-42-869-3714; fax: +82-42-869-3710.

E-mail address: swbaek@sorak.kaist.ac.kr (S.W. Baek).

0017-9310/01/$ - see front matter
PII: S0017-9310(00)00270-2

Nomenclature

C_p	specific heat at constant pressure
I	radiative intensity
n_p	number density of particles
q^C	conductive heat flux
q^R	radiative heat flux
t	time
T	temperature

Greek symbols

δ	relative specific heat $(= C_{p,p}/C_{p,g})$
η	loading ratio $(= \sigma_p/\sigma_g)$
θ	dimensionless temperature
κ	absorption coefficient
λ	conductivity
μ	direction cosine
σ	concentration
σ_B	Stefan–Boltzmann constant
σ_s	scattering coefficient
τ_R	optical thickness $(= \beta R)$

Superscript

$*$	dimensionless quantity

Subscripts

m	mean value
g	gas phase
p	particle phase
0	reference value

both radiation and conduction redistribute the thermal energy. The energy equations are discretized using the implicit finite volume method, while the RTE is solved by using the discrete ordinates method (DOM). For a more systematic analysis of combined heat transfer in gas–particle two-phase medium, the effects of such thermal parameters as the conduction-to-radiation parameter, optical thickness, convection-to-radiation parameter, gas and particle absorption-to-extinction ratio, wall emissivity and heat capacity ratio are sought. Actually, the combined heat transfer problem in a gas–particle two-phase medium is so complicated that such a systematic approach is essential. A complete two-phase radiation due to gas and particles is now considered, which is different from the previous studies and to our best knowledge, it has not been done yet.

2. Analysis

2.1. Governing equations

The present study focuses on the transient cooling of hot two-phase medium of radius R which is instantaneously exposed to the cold rarefied environment as is shown in Fig. 1. The boundary wall is fixed and its emissivity can be adjusted to satisfy the heat balance of the overall system by changing the coating substance [8] and the two-phase medium is initially at uniform temperature T_0. At the boundary the medium emits the energy by radiation only, whereas the conduction and radiation interact to internally redistribute thermal energy. Since only the radiative heat loss to the surrounding is assumed, there would be no conductive or convective energy transfer to the surrounding at the boundary. The incoming radiation from the surrounding is neglected due to its very low temperature.

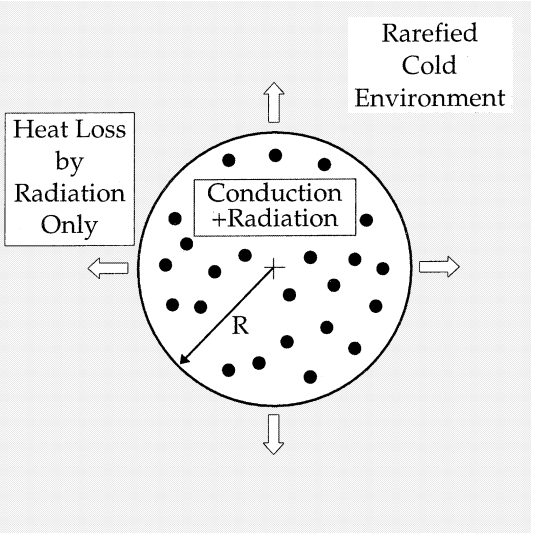

Fig. 1. Schematic of the problem.

Under the above physical consideration and assumption of constant physical properties, the gas and particle energy conservation equations considering the conductive and radiative heat transfers can be expressed as follows:

gas energy equation

$$\sigma_g C_{p,g} \frac{\partial T_g}{\partial t} = \frac{\lambda_g}{r^2} \frac{\partial}{\partial r}\left(r^2 \frac{\partial T_g}{\partial r}\right) + hA_s n_p (T_p - T_g) - \nabla \cdot \vec{q}_g^R, \tag{1}$$

particle energy equation

$$\sigma_p C_{p,p} \frac{\partial T_p}{\partial t} = hA_s n_p (T_g - T_p) - \nabla \cdot \vec{q}_p^R, \tag{2}$$

where the divergence of radiative heat flux for gas and particles are, respectively, given by [7]

$$\nabla \cdot \vec{q}_{\mathrm{g}}^{\mathrm{R}} = \kappa_{\mathrm{g}}\left(4\pi I_{\mathrm{bg}} - \int_{4\pi} I \,\mathrm{d}\Omega\right), \tag{3a}$$

$$\nabla \cdot \vec{q}_{\mathrm{p}}^{\mathrm{R}} = \kappa_{\mathrm{p}}\left(4\pi I_{\mathrm{bp}} - \int_{4\pi} I \,\mathrm{d}\Omega\right). \tag{3b}$$

The energy from the inner region can pass through the outer boundary only by radiation, for the boundary of the medium joining the rarefied surrounding is externally insulated with regard to the conduction portion of the energy transfer. Therefore, the boundary condition at outer boundary at R for Eq. (1) is zero temperature gradient. At the center of the medium in spherical shape, the symmetric condition is imposed so that

$$\frac{\partial T_{\mathrm{g}}}{\partial r} = 0 \quad \text{at } r = 0 \text{ and } R. \tag{4}$$

The boundary conditions for the particle energy equation are not necessary, because once the local gas temperature is determined, the particle temperature can be subsequently calculated using the particle energy equation, Eq. (2).

2.2. Radiative transfer equation

To analyze the radiation in two-phase medium in a sphere, a mixture of the gas and particles is assumed to be gray, but their temperatures are different, i.e., at thermal nonequilibrium. For a gray, emitting, absorbing and isotropically scattering two-phase medium in thermal nonequilibrium, the RTE can be written by [7]

$$\mu\frac{\partial I}{\partial r} + \frac{1-\mu^2}{r}\frac{\partial I}{\partial \mu} + (\kappa_{\mathrm{g}} + \kappa_{\mathrm{p}} + \sigma_{\mathrm{s}})I = \kappa_{\mathrm{g}} I_{\mathrm{bg}} + \kappa_{\mathrm{p}} I_{\mathrm{bp}} + \frac{\sigma_{\mathrm{s}}}{2}\int_{-1}^{1} I(r,\mu_i)\,\mathrm{d}\mu_i, \tag{5}$$

where I_{bg} and I_{bp} are the blackbody emissive power corresponding to each local temperature for the gas and particles, respectively. As noted in the above equation, while all of the emission, absorption, and scattering are considered for the particles, the scattering for the gas is neglected. Furthermore, it is noted that the time derivative term of the radiative intensity is neglected, since it is smaller than the other terms by speed of light. The boundary condition for the outer wall, which is assumed to be a diffusely reflecting and emitting one, is given by

$$I_{\mathrm{w}} = \varepsilon_{\mathrm{w}} I_{\mathrm{bg,w}} + \frac{1-\varepsilon_{\mathrm{w}}}{\pi}\int_{\hat{n}_{\mathrm{w}}\cdot\hat{s}_i<0} I(\hat{s}_i)\left|\hat{n}_{\mathrm{w}}\cdot\hat{s}_i\right|\mathrm{d}\Omega_i \quad \text{for } \hat{n}_{\mathrm{w}}\cdot\hat{s}_i > 0 \tag{6}$$

where ε_{w} is the wall emissivity and $\hat{n}_{\mathrm{w}}$ is the unit normal vector to the wall. The contribution to the radiative intensity by particles at the wall is neglected, since the particle volume fraction therein is negligible. The symmetric condition is imposed at the center of medium such that

$$I = I' \quad \text{for } \mu = -\mu' \text{ at } r = 0 \tag{7}$$

2.3. Nondimensionalization

Two energy equations (1) and (2) and the radiative transfer equation (5) can be nondimensionalized as follows:

$$\frac{\partial \theta_{\mathrm{g}}}{\partial t^*} = N_{\mathrm{CR}}\frac{1}{r^{*2}}\frac{\partial}{\partial r^*}\left(r^{*2}\frac{\partial \theta_{\mathrm{g}}}{\partial r^*}\right) + N_{\mathrm{VR}}(\theta_{\mathrm{p}} - \theta_{\mathrm{g}}) - \bar{\omega}_{\mathrm{g}}\tau_{\mathrm{R}}\left(\theta_{\mathrm{g}}^4 - \frac{1}{2}\int_{-1}^{1} I^*\,\mathrm{d}\mu\right) \tag{8}$$

$$\delta\eta\frac{\partial \theta_{\mathrm{p}}}{\partial t^*} = N_{\mathrm{VR}}(\theta_{\mathrm{g}} - \theta_{\mathrm{p}}) - \bar{\omega}_{\mathrm{p}}\tau_{\mathrm{R}}\left(\theta_{\mathrm{p}}^4 - \frac{1}{2}\int_{-1}^{1} I^*\,\mathrm{d}\mu\right) \tag{9}$$

$$\frac{1}{\tau_{\mathrm{R}}}\left(\mu\frac{\partial I^*}{\partial r^*} + \frac{1-\mu^2}{r^*}\frac{\partial I^*}{\partial \mu}\right) + I^* = \bar{\omega}_{\mathrm{g}}\theta_{\mathrm{g}}^4 + \bar{\omega}_{\mathrm{p}}\theta_{\mathrm{p}}^4 + \frac{\omega_{\mathrm{s}}}{2}\int_{-1}^{1} I^*(r^*,\mu_i)\,\mathrm{d}\mu_i \tag{10}$$

by introducing the dimensionless variables and parameters:

$$\begin{aligned}
&\theta_{\mathrm{g}} = \frac{T_{\mathrm{g}}}{T_0}, \quad \theta_{\mathrm{p}} = \frac{T_{\mathrm{p}}}{T_0}, \quad r^* = \frac{r}{R}, \quad t^* = \frac{4\sigma_{\mathrm{B}}T_0^3}{\sigma_{\mathrm{g}}C_{\mathrm{p,g}}R}t, \quad I^* = \frac{\pi I}{\sigma_{\mathrm{B}}T_0^4}\\
&N_{\mathrm{CR}} = \frac{\lambda_{\mathrm{g}}}{4\sigma_{\mathrm{B}}T_0^3R}, \quad N_{\mathrm{VR}} = \frac{hA_{\mathrm{s}}n_{\mathrm{p}}R}{4\sigma_{\mathrm{B}}T_0^3},\\
&\tau = \beta r, \quad \tau_{\mathrm{R}} = \beta R, \quad \beta = \kappa_{\mathrm{g}} + \kappa_{\mathrm{p}} + \sigma_{\mathrm{s}},\\
&\omega_{\mathrm{s}} = \frac{\sigma_{\mathrm{s}}}{\kappa_{\mathrm{g}} + \kappa_{\mathrm{p}} + \sigma_{\mathrm{s}}}, \quad \bar{\omega}_{\mathrm{g}} = \frac{\kappa_{\mathrm{g}}}{\kappa_{\mathrm{g}} + \kappa_{\mathrm{p}} + \sigma_{\mathrm{s}}},\\
&\bar{\omega}_{\mathrm{p}} = \frac{\kappa_{\mathrm{p}}}{\kappa_{\mathrm{g}} + \kappa_{\mathrm{p}} + \sigma_{\mathrm{s}}}.
\end{aligned} \tag{11}$$

In the above expressions N_{CR} is the conduction-to-radiation parameter and N_{VR} is the convection-to-radiation parameter, while β is the overall extinction coefficient by gas and particles. Similar to the definition of the scattering albedo, ω_{s}, the parameters $\bar{\omega}_{\mathrm{g}}$ and $\bar{\omega}_{\mathrm{p}}$ are newly defined as above in Eq. (11) and named as the gas absorption-to-extinction ratio and the particle absorption-to-extinction ratio, respectively. Physically, each absorption-to-extinction ratio represents the relative importance of absorption or emission by gas or particles.

2.4. Supplementary relations

Since particles are discretely distributed in the gas medium, the total heat flux along the radial direction consists of conductive and radiative heat fluxes as follows:

$$q^* = \frac{q_{\mathrm{g}}^C + q^{\mathrm{R}}}{\sigma_{\mathrm{B}}T_0^4} = -\frac{4N_{\mathrm{CR}}}{\tau_{\mathrm{R}}}\frac{\partial \theta_{\mathrm{g}}}{\partial r^*} + \frac{1}{\pi}\int_{4\pi} I^*(\hat{n}\cdot\hat{s})\,\mathrm{d}\Omega, \tag{12}$$

In order to evaluate the respective contributions of radiation by gas and particles to each type of energy equation, the dimensionless form of the divergence of radiative heat flux for each phase can be denoted by

$$\left(\nabla \cdot q_{\mathrm{g}}^{\mathrm{R}}\right)^{*} = 4\bar{\omega}_{\mathrm{g}}\tau_{\mathrm{R}}\left(\theta_{\mathrm{g}}^{4} - \frac{1}{4\pi}\int_{4\pi} I^{*}\,\mathrm{d}\Omega\right), \tag{13}$$

$$\left(\nabla \cdot q_{\mathrm{p}}^{\mathrm{R}}\right)^{*} = 4\bar{\omega}_{\mathrm{p}}\tau_{\mathrm{R}}\left(\theta_{\mathrm{p}}^{4} - \frac{1}{4\pi}\int_{4\pi} I^{*}\,\mathrm{d}\Omega\right). \tag{14}$$

The dimensionless gas and particle mean temperatures across the medium can be defined as

$$\theta_{\mathrm{g,m}} = \int_{0}^{1} \theta_{\mathrm{g}}(r^{*})^{2}\,\mathrm{d}r^{*}, \tag{15a}$$

$$\theta_{\mathrm{p,m}} = \int_{0}^{1} \theta_{\mathrm{p}}(r^{*})^{2}\,\mathrm{d}r^{*} \tag{15b}$$

which implies the ratio of the remaining energy at any time to the initial energy in each phase. This is convenient to describe the cooling behavior of the system.

3. Numerical methods

The gas and particle energy equations (1) and (2) are discretized and solved using the implicit finite volume method [9]. Because of strong nonlinearlity of the radiative flux, special care must be taken on the radiative divergence terms in Eqs. (1) and (2) to guarantee a good convergence of the solution.

The RTE, Eq. (5), is solved by using the DOM, which spans a full range of the total solid angle 4π only in a finite number of ordinates directions with corresponding direction cosines μ^{m} and weighting factors w^{m}. Since the derivation of discretized form of RTE is already described before [1,10], its detailed procedure is omitted here for brevity. The resulting expression for the radiative intensity at a local point P in the mth directional ordinate is obtained as follows:

$$\begin{aligned} I_{P}^{m} = &\Big\{4|\mu_{m}|(AI)_{P}^{m} + 2(A_{n}-A_{\mathrm{s}})/w_{m}\big[f\alpha_{m-1/2} \\ &+ (1-f)\alpha_{m+1/2}\big]I_{P}^{m-1/2} + 4fS(r^{*},\mu_{m})V\Big\}\Big/\big\{2|\mu_{m}|A_{\mathrm{se}} \\ &+ 2(A_{n}-A_{\mathrm{s}})/w_{m}\big(\alpha_{m+1/2}+\alpha_{m-1/2}\big) + 4f\tau_{\mathrm{R}}V\big\} \end{aligned} \tag{16}$$

with

$$(AI)_{P}^{m} = \begin{cases} [A_{e}(1-f)+A_{\mathrm{w}}f]I_{\mathrm{w}}^{m} & \text{for } \mu_{m}>0, \\ [A_{\mathrm{w}}(1-f)+A_{e}f]I_{e}^{m} & \text{for } \mu_{m}<0, \end{cases} \tag{17}$$

$$A_{\mathrm{se}} = \begin{cases} A_{n} & \text{for } \mu_{m}>0, \\ A_{\mathrm{s}} & \text{for } \mu_{m}<0, \end{cases} \tag{18}$$

$$S(r^{*},\mu_{m}) = \tau_{\mathrm{R}}\left[\bar{\omega}_{\mathrm{g}}I_{\mathrm{bg}}^{*} + \bar{\omega}_{\mathrm{p}}I_{\mathrm{bp}}^{*} + \frac{\omega_{\mathrm{s}}}{4\pi}\sum_{m_{i}=1}^{M} w_{m_{i}}I_{P}^{*m_{i}}\right], \tag{19}$$

$$V = 4\pi/3\left(r_{n}^{*3} - r_{\mathrm{s}}^{*3}\right), \quad A_{n} = 4\pi r_{n}^{*2}, \quad A_{\mathrm{s}} = 4\pi r_{\mathrm{s}}^{*2}, \tag{20}$$

where $\alpha_{m+1/2}$ is a coefficient for the angular derivative term and f is an interpolating coefficient for two facial intensities in one cell which is determined to prevent a negative intensity from occurring at P. The boundary condition for the outer wall embedded in DOM is

$$I_{\mathrm{w}} = \varepsilon_{\mathrm{w}}I_{\mathrm{bg,w}} + 1 - \varepsilon_{\mathrm{w}}/\pi \sum_{\hat{n}_{\mathrm{w}}\cdot\hat{s}_{i}<0} w_{m}I^{*}\left(r_{\mathrm{w}}^{*},\hat{s}_{i}\right)\left|\hat{n}_{\mathrm{w}}\cdot\hat{s}_{i}\right| \tag{21}$$

for $\hat{n}_{\mathrm{w}}\cdot\hat{s}_{i}>0$.

A numerical procedure starts by solving the RTE with an initially assumed temperature distribution at one time step. Then, the divergence for radiative heat flux for gas and particles is calculated and substituted into the two energy equations. Thereby, a new temperature field is obtained. This process is repeated until the following convergence criterion is satisfied for all variables;

$$\left|\frac{\phi_{i,j}^{n+1} - \phi_{i,j}^{n}}{\phi_{i,j}^{n+1}}\right| < 10^{-6}, \tag{22}$$

where ϕ is θ_{g} or θ_{p} and the iteration step is denoted by n. Then, the numerical procedure proceeds to the next time step.

In order to verify the present program for solving radiation, a nonscattering benchmark solution is considered, which is a problem of combined conduction and radiation between two concentric cold black spherical boundaries separated by radiating medium with uniform temperature. In Fig. 2, the numerical solutions for radiative heat flux are presented for various absorption coefficients and compared with the analytical ones by Viskanta and Merriam [11]. The present S_{6} results are in

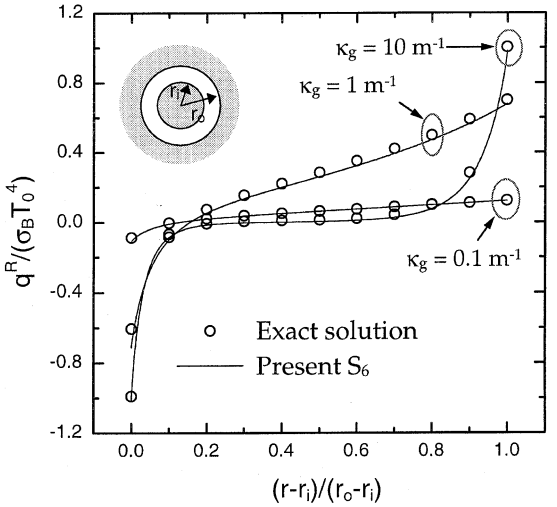

Fig. 2. Comparision of the present DOM (S_{6}) with exact solution.

good agreement with analytical ones so that a higher order approximation than S_6 would not be necessary.

4. Results and discussion

Unless otherwise specified, all the calculations presented below are carried out for the following conditions; conduction-to-radiation parameter $N_{CR} = 1$; convection-to-radiation parameter $N_{VR} = 1$; optical thickness $\tau_R = 1$; gas absorption-to-extinction ratio $\bar{\omega}_g = 0.3$; particle absorption-to-extinction ratio $\bar{\omega}_p = 0.3$; outer boundary emissivity $\varepsilon_w = 1$; a ratio of specific heat for particle to that for gas $\delta = 100$; a mass loading ratio of particle to gas $\eta = 0.01$. Since the scattering effect in cooling problem is previously discussed [12,13], its effect is not examined here and ω_s is set to be 0.4. The initial dimensionless temperatures for gas θ_g and particles θ_p are assumed to be 1.

Fig. 3(a) illustrates a transient temperature variation along radial direction for various conduction-to-radiation parameters, N_{CR} while the other parameters are fixed. Since the two-phase medium is exposed to the rarefied cold environment, the internal energy of the spherical medium begins to decrease due to the radiative loss at the boundary. As the medium cools down near the boundary, the temperature gradient is created therein. As N_{CR} increases, the gas temperature becomes more uniform at each dimensionless time step, for the stronger conduction plays a role in smoothening out the temperature gradient. However, the effect of the conduction-to-radiation parameter, N_{CR} on the particle temperature is seen to be minor in the figure, since it usually occurs through the convection-to-radiation parameter, N_{VR} between gas and particles which is now a constant value of 1. In the figure, the particle temperature near the boundary is shown to be lower than the gas temperature. This results from the fact that the two-phase medium at the boundary cools down due to radiative heat loss only to the rarefied environment, but the gas at boundary is heated up by the conduction. That is also why the gas temperature deeper inside the sphere is lower than the particle temperature.

In order to better understand the combined conduction and radiation, a transient variation of conductive, radiative and total heat fluxes is plotted in Fig. 3(b). The fact, which is common to all the figures, is that the radiative heat flux is much more dominant over the conductive one for the conditions given as seen in the scale in figures. Furthermore, the radiative heat flux is shown to continuously decrease as time goes on, while the conductive heat flux shows a different behavior. For the case for $N_{CR} = 0.01$, the conductive heat flux invariably increases as time passes. Consequently, the position of the maximum temperature gradient migrates into the inner region with its value getting larger. On the other hand, as N_{CR} increases, the conductive behavior changes such that the conductive heat flux initially increases and then decreases, since the conduction plays a more significant role for larger N_{CR}.

The local radiative heat loss per unit volume in gas and particle phases can be described in terms of the divergence of radiative heat flux for gas and particles, respectively. Their temporal variations are plotted in Fig. 3(c). In the inner region of medium, $\nabla \cdot \vec{q}_p^R$ is larger than $\nabla \cdot \vec{q}_g^R$, which means that the net radiative flux for particle phase out of corresponding control volume is larger than that for gas phase. But therein, the energy in gas phase is transferred by conduction as well as by radiation while the conductive heat flux increases reaching its maximum as shown in Fig. 3(b). On the other hand, the particle phase has only one heat transfer mechanism so that the gas temperature becomes lower than the particle temperature in inner region. Different from the inner region, at the vicinity of the boundary adjoining the rarefied cold environment, the conduction in gas phase decreases to zero so that the heat delivered from inner region is converted to radiant energy. This leads to the fact that the divergence of radiative flux for gas phase becomes larger than that for particle phase as shown in Fig. 3(c).

The effects of convection exchange between gas and particles are investigated in Fig. 4(a). The values used for convection-to-radiation parameter are $N_{VR} = 0.1, 1$ and 10. As N_{VR} increases, the local temperature difference rapidly decreases due to the stronger thermal interaction between two phases. Similar to the effects of N_{CR} mentioned above, N_{VR} is found to affect the internal temperature distribution only in the system, while the other thermal characteristics such as the total heat loss to cold environment and the mean temperature variations remain nearly unchanged. For example, the temporal variations of the particle and gas mean temperature are almost the same regardless of N_{VR} as presented in Fig. 4(b). These mean temperatures actually imply a residual energy left in the sphere.

In Fig. 5(a), the effects of optical thickness on the temporal variation of gas and particle temperatures are plotted for $\tau_R = 0.5, 1$ and 10. For a small optical thickness of $\tau_R = 0.5$, the temperature distribution is seen to be uniform except for the particle temperature near the outer boundary. However, as τ_R increases, more energy is emitted to the surrounding cold environment so that the gas temperature more rapidly decreases approaching to the outer boundary. Simultaneously, the particle temperature conspicuously drops near the boundary. Thereby, the gas temperature gradient increases, which then results in an increase of the conductive heat flux in gas phase as in Fig. 5(b). In this figure it is also observed that the total heat flux at the outer boundary is the largest for $\tau_R = 10$ initially. However, as time passes, it quickly reduces, since the temperature therein decreases as seen in Fig. 5(a).

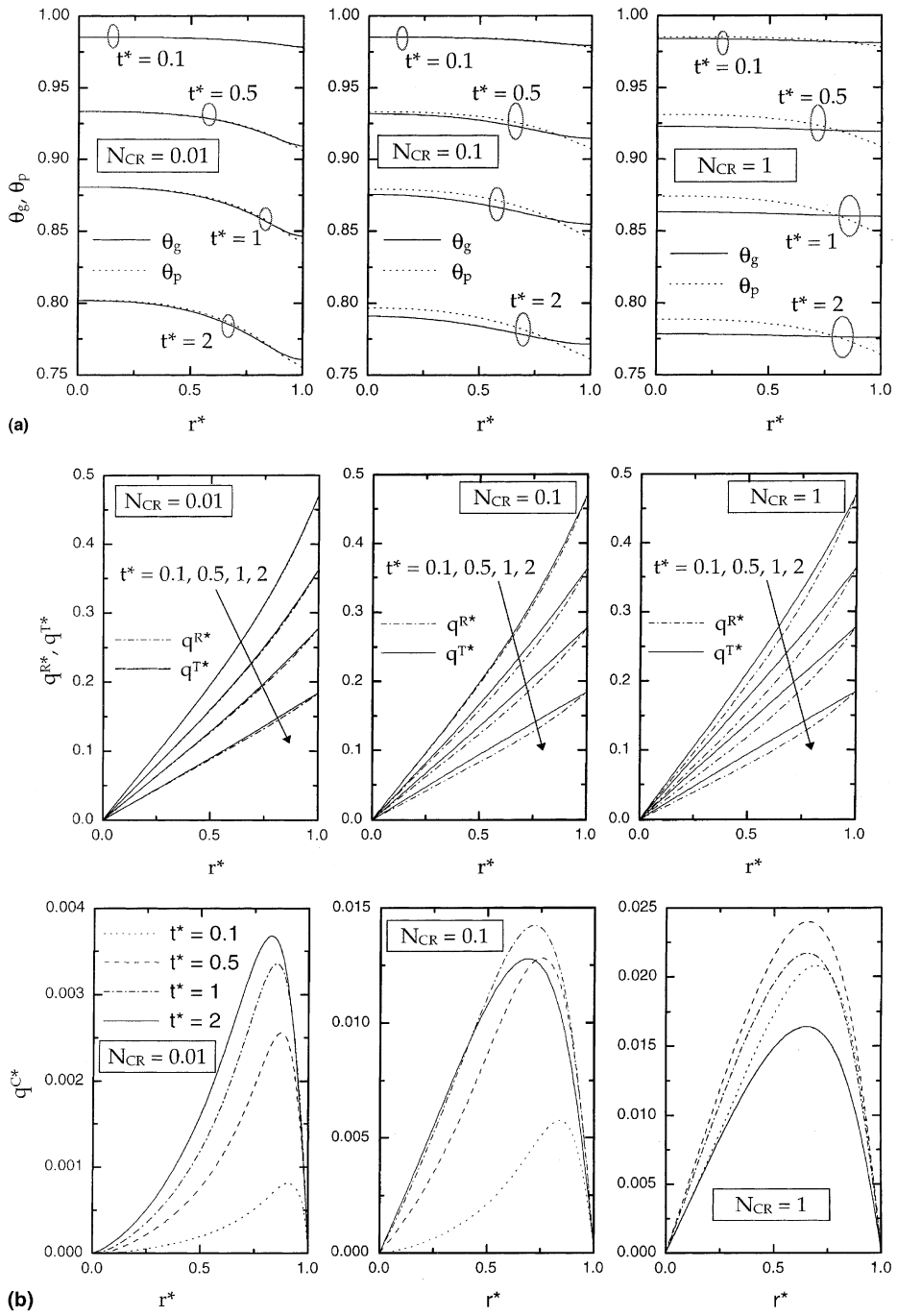

Fig. 3. (a) Transient gas and particle temperature variations along radial direction for various N_{CR} for $N_{VR} = 1$, $\tau_R = 1$, $\bar{\omega}_g = 0.3$, $\bar{\omega}_p = 0.3$, $\delta = 100$ and $\eta = 0.01$. (b) Transient conductive, radiative, and total heat flux variations along radial direction for various N_{CR} for $N_{VR} = 1$, $\tau_R = 1$, $\bar{\omega}_g = 0.3$, $\bar{\omega}_p = 0.3$, $\delta = 100$, and $\eta = 0.01$. (c) Transient variations of divergence of radiative heat flux along radial direction for various N_{CR} for $N_{VR} = 1$, $\tau_R = 1$, $\bar{\omega}_g = 0.3$, $\bar{\omega}_p = 0.3$, $\delta = 100$, and $\eta = 0.01$.

In Fig. 5(c), the corresponding gas and particle mean temperature variations are drawn to compare an overall cooling rate for various τ_R. As τ_R increases, the medium near the outer boundary can emit more radiation into the cold environment. Therefore, the dimensionless mean temperature is lower for higher τ_R during the en-

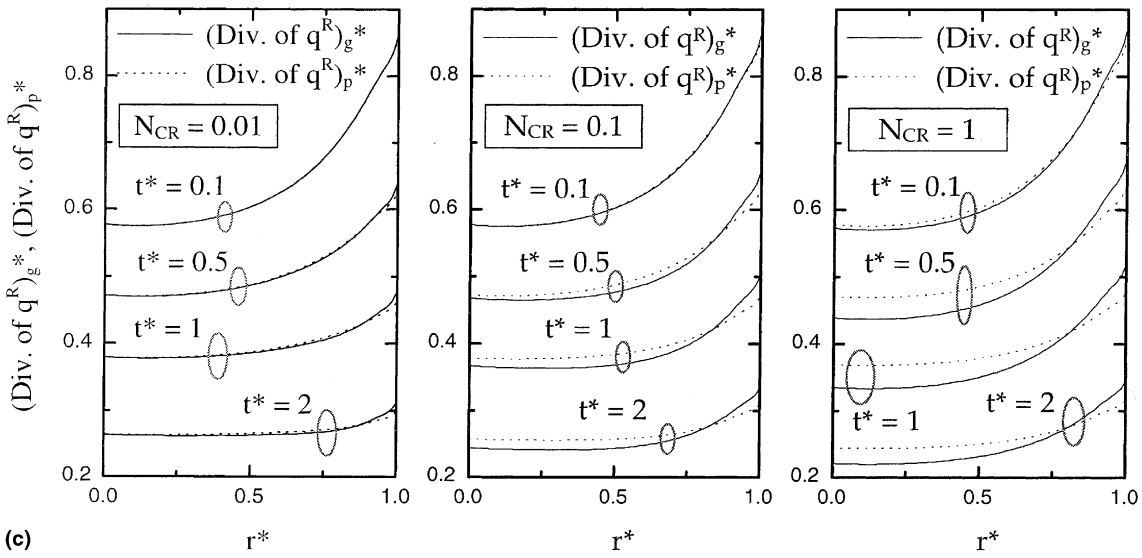

Fig. 3 (*continued*)

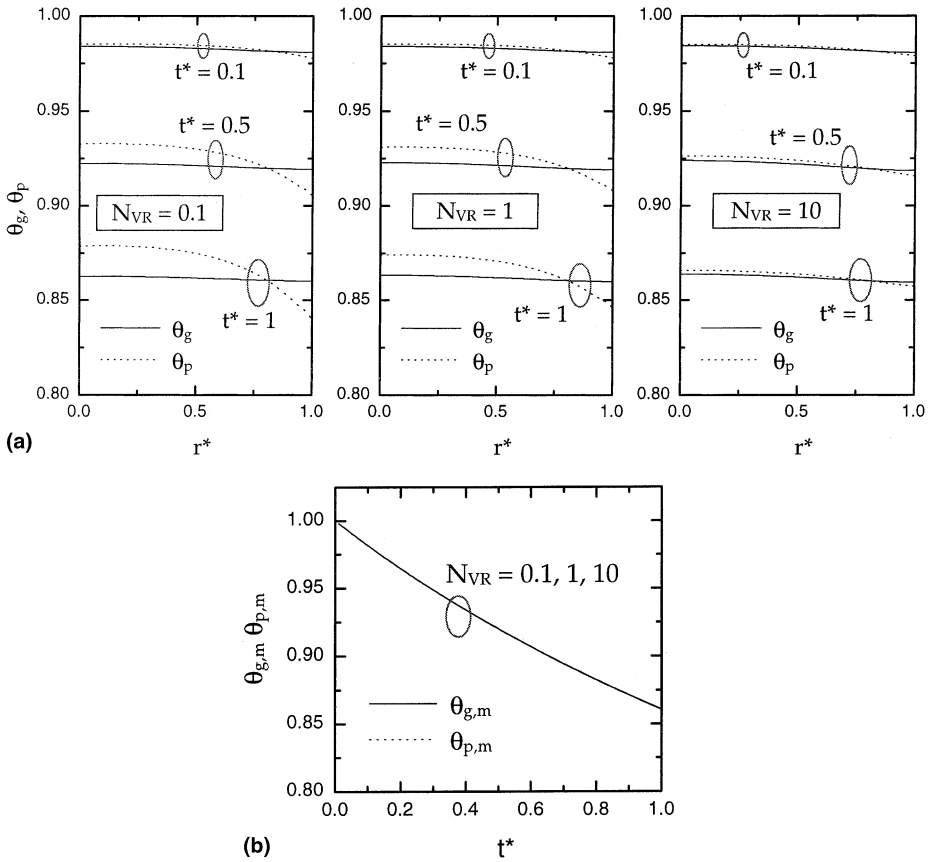

Fig. 4. (a) Transient gas and particle temperature variations along radial direction for various N_{VR} for $N_{CR} = 1$, $\tau_R = 1$, $\bar{\omega}_g = 0.3$, $\bar{\omega}_p = 0.3$, $\delta = 100$, and $\eta = 0.01$. (b) Transient gas and particle mean temperature variations for various N_{VR} for $N_{CR} = 1$, $\tau_R = 1$, $\bar{\omega}_g = 0.3$, $\bar{\omega}_p = 0.3$, $\delta = 100$, and $\eta = 0.01$.

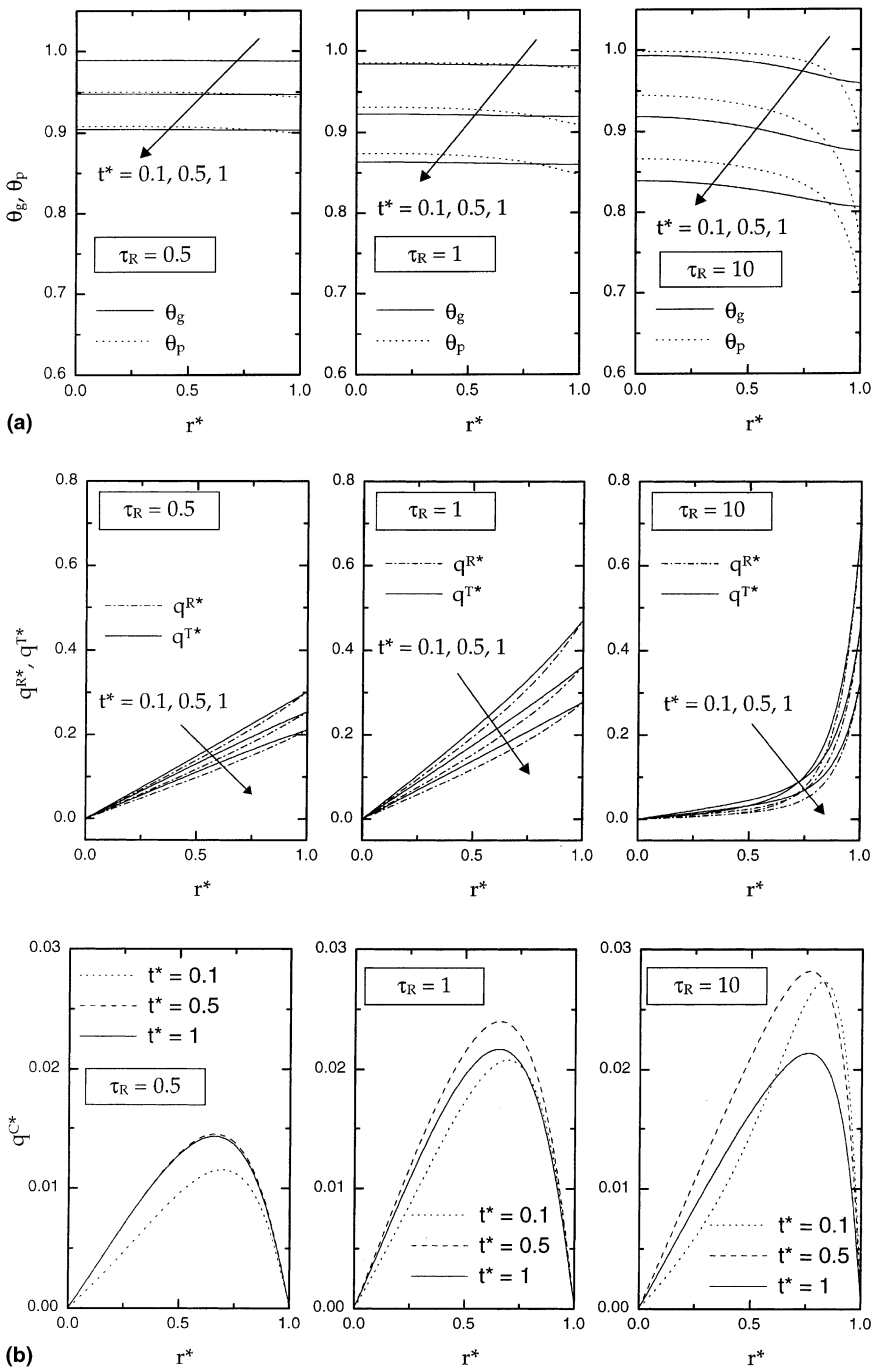

Fig. 5. (a) Transient gas and particle temperature variations along radial direction for various τ_R for $N_{CR} = 1$, $N_{VR} = 1$, $\bar{\omega}_g = 0.3$, $\bar{\omega}_p = 0.3$, $\delta = 100$, and $\eta = 0.01$. (b) Transient conductive, radiative, and total heat flux variations along radial direction for various τ_R for $N_{CR} = 1$, $N_{VR} = 1$, $\bar{\omega}_g = 0.3$, $\bar{\omega}_p = 0.3$, $\delta = 100$, and $\eta = 0.01$. (c) Transient gas and particle temperature variations for various τ_R for $N_{CR} = 1$, $N_{VR} = 1$, $\bar{\omega}_g = 0.3$, $\bar{\omega}_p = 0.3$, $\delta = 100$, and $\eta = 0.01$.

tire cooling time. While the gas and particle mean temperatures are almost the same for $\tau_R = 1$ and 10, the particle mean temperature for $\tau_R = 0.5$ is seen to be a bit lower than the gas mean temperature for the conditions of $\bar{\omega}_g = \bar{\omega}_p$ and $\eta\delta = 1$. In addition, the gas temperature gradient in the present study is found to be far smaller

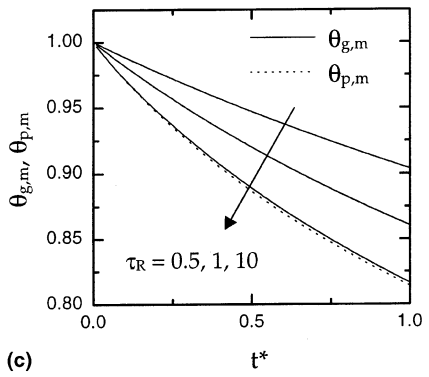

Fig. 5 (*continued*)

than that for the cooling problem of gas only medium [14], since the radiative heat loss by gas phase becomes smaller due to the partial allotment of the total radiative heat loss into each phase in two-phase mixture.

As mentioned above, the absorption-to-extinction ratio of each phase represents the emitting fraction of total radiation by gas or particles. Figs. 6(a) and (b) illustrate the transient temperature variations for $(\bar{\omega}_g, \bar{\omega}_p) = (0.1, 0.5), (0.3, 0.3)$, and $(0.5, 0.1)$. In Fig. 6(a) it is found that a phase with the larger absorption-to-extinction ratio emits more heat and cools down faster. It is also observed in the figure that as $\bar{\omega}_p$ increases, the radiative heat flux in gas phase decreases while the total heat flux in the system is not changing. That is why a severe temperature gradient in particle phase is induced as seen in Fig. 6(a). Besides, the particle temperature is seen to respond more sensitively to the variation of particle absorption-to-extinction ratio due to the lack of conduction than the gas temperature does to the variation of gas absorption-to-extinction ratio.

In Fig. 6(b) the mean temperature corresponding to the phase with larger absorption-to-extinction ratio is clearly seen to decrease faster as time goes on. Consequently, when the ratio of $\bar{\omega}_g/\bar{\omega}_p = 0.2$, the particle mean temperature is much lower than the gas mean temperature and vice versa for $\bar{\omega}_g/\bar{\omega}_p = 5.0$. On the other hand, when $\bar{\omega}_g/\bar{\omega}_p = 1.0$, two mean temperatures are seen to be overlapped against time. A similar variation in two mean temperature variations are shown in the figure such that the transient behavior in $\theta_{g,m}$ for

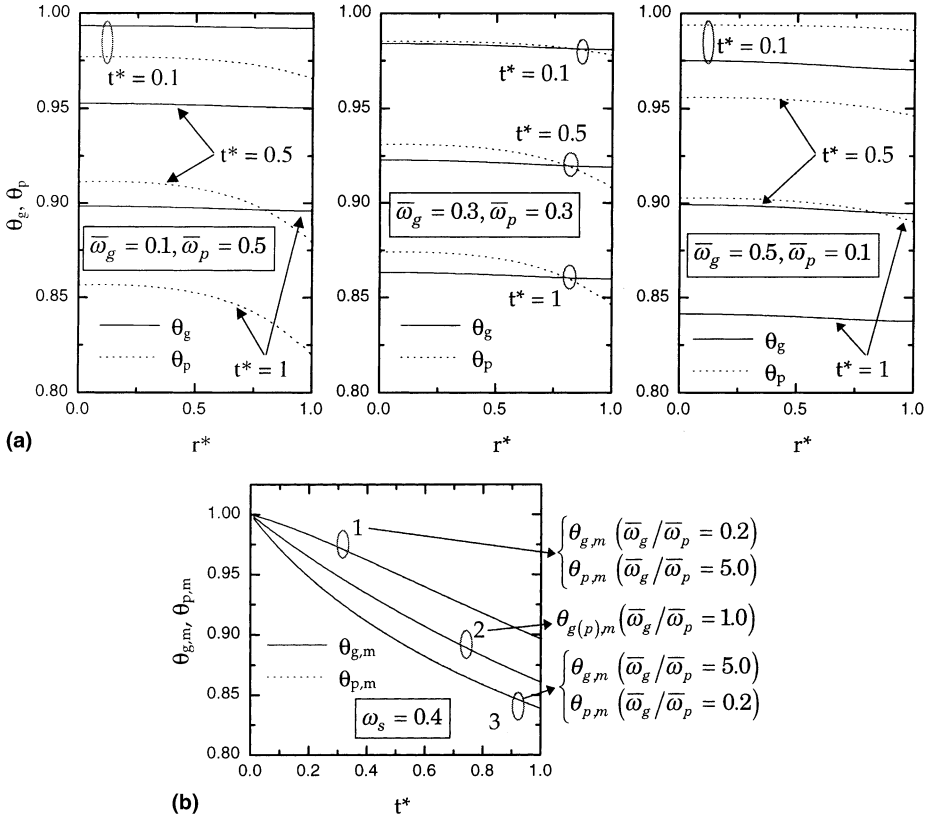

Fig. 6. (a) Transient gas and particle temperature variations along radial direction for various combinations of $\bar{\omega}_g$ and $\bar{\omega}_p$ for $N_{CR} = 1$, $N_{VR} = 1$, $\tau_R = 1$, $\delta = 100$ and $\eta = 0.01$. (b) Transient gas and particle mean temperature variations for various combinations of $\bar{\omega}_g$ and $\bar{\omega}_p$ for $N_{CR} = 1$, $N_{VR} = 1$, $\tau_R = 1$, $\delta = 100$, and $\eta = 0.01$.

$(\bar{\omega}_g, \bar{\omega}_p) = (0.1, 0.5)$ is nearly equal to that in $\theta_{p,m}$ for $(\bar{\omega}_g, \bar{\omega}_p) = (0.5, 0.1)$. It also applies to the variations of $\theta_{p,m}$ for $(\bar{\omega}_g, \bar{\omega}_p) = (0.5, 0.1)$ and $\theta_{g,m}$ for $(\bar{\omega}_g, \bar{\omega}_p) = (0.1, 0.5)$. This is because $\eta\delta = 1$ is used, which interprets that the heat capacity of gas phase is equal to that of particle phase.

The effect of outer boundary emissivity is plotted in Figs. 7 (a) and (b) for $\varepsilon_w = 0.8, 0.9$ and 1.0. When assuming no transmissivity, the emissivity $\varepsilon_w = 0.8, 0.9$ and 1.0 correspond to the reflectivity $\rho_w = 0.2, 0.1$ and 0.0. As the outer boundary emissivity decreases, the reflection of the incoming radiative intensity toward the inner medium increases so that more radiation is absorbed by the medium. This then results in the slower cooling of the medium as seen in Fig. 7(b) and leads to the more uniformization in temperature distribution as in Fig. 7(a). Moreover, due to the geometrical characteristics of sphere such that the volume of outer region is proportional to r^3, there exists the so-called 'volume effect' [9] so that the cooling rate of the medium drastically decreases with a decrease in ε_w or an increase in ρ_w. When ε_w is 0.75, the heat loss to the surrounding becomes almost negligible.

In Figs. 8(a)–(c), the effects of the heat capacity ratio, $\eta\delta$, on the cooling characteristics are shown. By definition, $\eta\delta = \sigma_p C_{p,p}/\sigma_g C_{p,g}$ represents a ratio of heat capacity of particle phase to that of gas phase. Fig. 8(a) illustrates the transient gas and particle temperature variations along radial direction while the transient radiative heat loss variation at outer boundary is drawn in Fig. 8(b) and the transient mean temperature variations are in Fig. 8(c). As $\eta\delta$ increases, especially the cooling rate in particle phase slows down as in Figs. 8(a) and (c), which then results in a decrease in gas phase cooling rate even though the magnitude of the radiative loss at the outer boundary increases as in Fig. 8(b). The reason for this is as follows. An increase in $\eta\delta$ brings about an increase in the heat capacity of the medium so that the rate of decrease in temperature decreases. Simultaneously, the temperature gradient in both phases decreases, which then leads to a reduction in conductive heat flux. The resulting higher temperature for higher $\eta\delta$ is then attributed to the higher radiative heat loss. In Fig. 8(c) it is also observed that when $\eta\delta = 1$, two mean temperature variations are almost the same. When $\eta\delta = 10$, the particle mean tem-

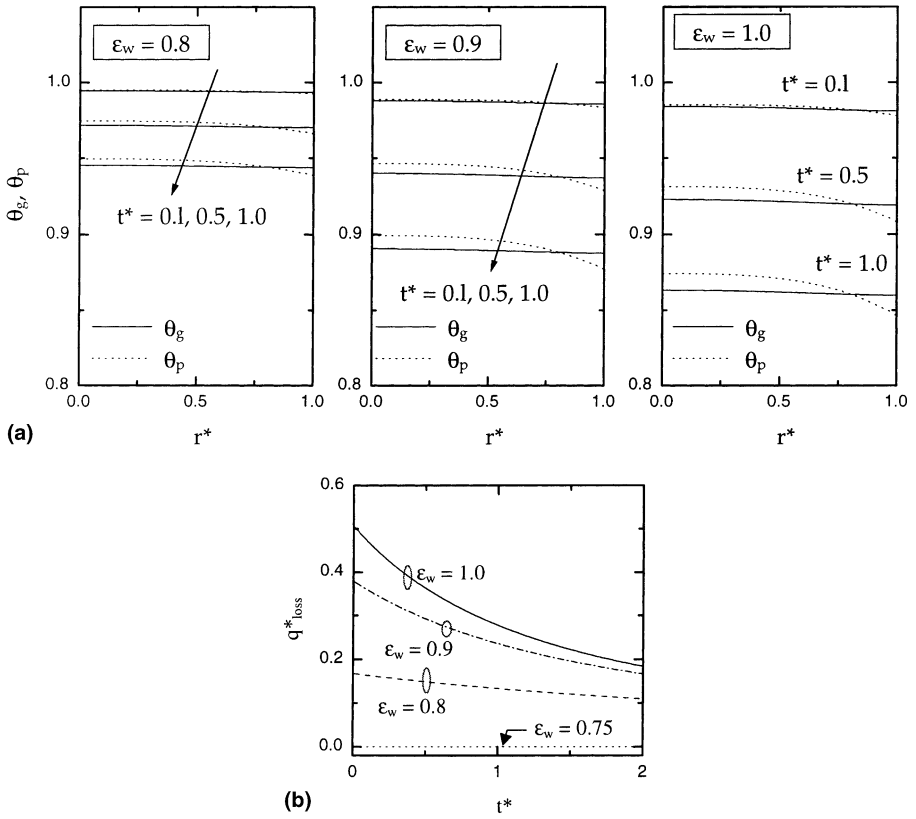

Fig. 7. (a) Transient gas and particle temperature variations along radial direction for various outer boundary emissivity, ϵ_w for $N_{CR} = 1$, $N_{VR} = 1$, $\tau_R = 1$, $\bar{\omega}_g = 0.3$, $\bar{\omega}_p = 0.3$, $\delta = 100$, and $\eta = 0.01$. (b) Radiative heat loss variations for various outer boundary emissivity, ϵ_w for $N_{CR} = 1$, $N_{VR} = 1$, $\tau_R = 1$, $\delta = 100$, and $\eta = 0.01$.

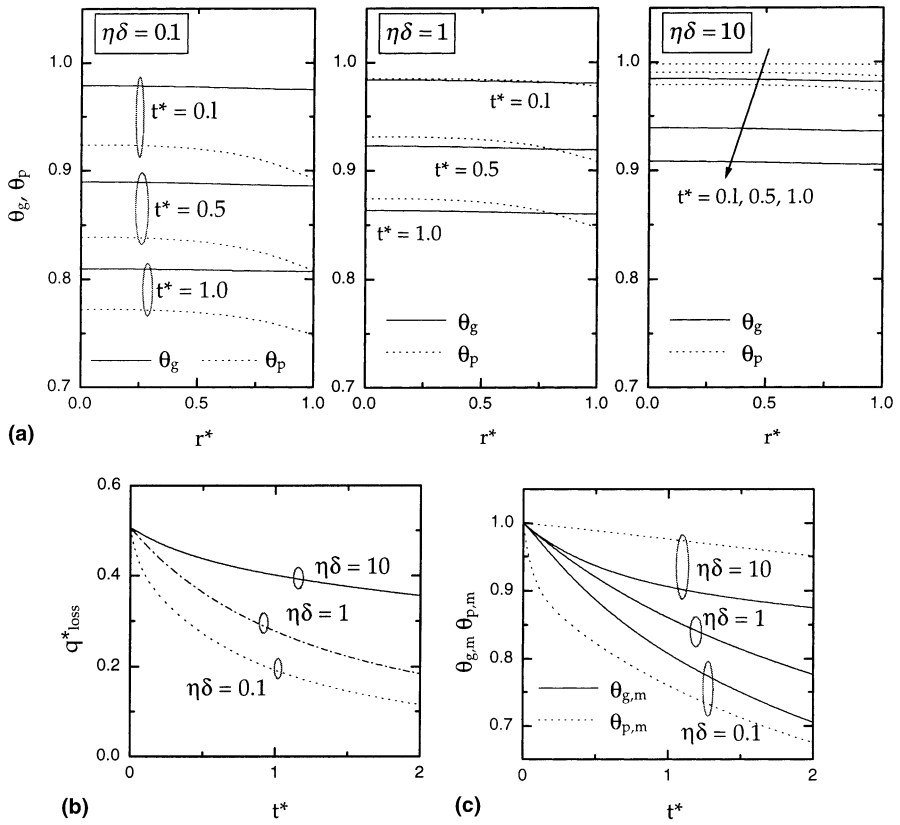

Fig. 8. (a) Transient gas and particle temperture variations along radial direction for various $\eta\delta$ for $N_{CR} = 1$, $N_{VR} = 1$, $\tau_R = 1$, $\bar{\omega}_g = 0.3$, $\bar{\omega}_p = 0.3$, $\delta = 100$, and $\eta = 0.01$. (b) Radiative heat loss variations for various $\tau\delta$ for $N_{CR} = 1$, $N_{VR} = 1$, $\tau_R = 1$, $\bar{\omega}_g = 0.3$, $\bar{\omega}_p = 0.3$. (c) Transient gas and particle mean temperature variations for various $\eta\delta$ for $N_{CR} = 1, N_{VR} = 1, \tau_R = 1, \bar{\omega}_g = 0.3, \bar{\omega}_p = 0.3$.

perature is seen to be higher than the gas mean temperature.

5. Concluding remarks

A numerical study is performed on the transient cooling phenomena of gas–particle two-phase medium in a spherical shape exposed to the rarefied cold environment. The DOM is used for solving the radiative transfer equation, while the finite volume method for the gas and particle energy equations. Especially, the two-phase radiative transfer equation, which takes account of absorption and emission by both gas and particles in addition to scattering by particles, is taken into consideration in this study. Its two-phase cooling characteristics are investigated for various parameters. The results obtained are as follows:

1. As N_{CR} increases, the gas temperature becomes more uniform, since the stronger conduction smoothens out the temperature gradient.
2. N_{VR} affects the internal thermal structures only while the overall mean temperature variation is the same, since the entire heat loss to surrounding occurs by radiation only.
3. As τ_R increases, the radiative heat loss near the boundary increases due to the larger emission.
4. The phase with a larger absorption-to-extinction ratio cools down more rapidly and the particle temperature responds more sensitively to the variation of absorption-to-extinction ratios.
5. As ε_w decreases, the energy loss to the surrounding rapidly decreases so that the cooling process slows down.
6. For a higher $\eta\delta$, the heat capacity of the medium becomes larger so that the slower cooling rate results even if the radiative heat loss at the outer boundary is higher.

Acknowledgements

This work was supported by Brain Korea 21 Project.

References

[1] I.H. Cho, S.W. Baek, S.H. Han, Unsteady cooling of a solid sphere in a radiatively active medium, Numer. Heat Transfer A34 (1998) 119–133.
[2] P.D. Jones, Y. Bayazitoglu, Combined radiation and conduction from sphere in a participating medium, in: Proceedings of the Ninth International Heat Transfer Conference, vol. 6, Hemisphere, Washington, DC, 1990, pp. 397–402.
[3] H. Tamehiro, R. Echigo, S. Hasegawa, Radiative heat transfer by flowing multiphase medium – part III. An analysis on heat transfer of turbulent flow in a circular tube, Int. J. Heat Mass Transfer 16 (1973) 1199–1213.
[4] K.M. Kim, H.J. Lee, S.W. Baek, Analysis of two-phase radiation in thermally developing poiseuille flow, Numer. Heat Transfer A36 (1999) 489–510.
[5] D.G. Gilmore (Ed.), Radiators, Satellite Thermal Control Handbook, The Aerospace Cooperation Press, El Segundo, CA, 1994 (Chapter 4).
[6] R.T. Taussig, A.T. Mattick, Droplet radiator systems for spacecraft thermal control, J. Spacecraft Rockets 23 (1986) 10–17.
[7] J.H. Park, S.W. Baek, S.J. Kwon, Analysis of a gas–particle direct-contact heat exchanger with two-phase radiation effect, Numer. Heat Transfer A 33 (1998) 701–721.
[8] D.G. Gilmore, W.K. Stuckey, Thermal surface finishes, in: D.G. Gilmore (Ed.), Satellite Thermal Control Handbook, The Aerospace Cooperation Press, El Segundo, CA, 1994 (Chapter 4).
[9] S.V. Patankar, Numerical Heat Transfer and Fluid Flow, Hemisphere, New York, 1980.
[10] S.W. Baek, J.H. Park, C.E. Choi, Investigation of droplet combustion with nongray gas radiation effects, Combust. Sci. Technol. 142 (1999) 55–76.
[11] R. Viskanta, R.L. Merriam, Heat transfer by combined conduction radiation between concentric spheres separated by radiating medium, J. Heat Transfer 90 (1968) 248–256.
[12] S.W. Baek, T.Y. Kim, J.S. Lee, Transient cooling of a finite cylindrical medium in the rarefied cold environment, Int. J. Heat Mass Transfer 36 (1993) 3949–3956.
[13] C. Yao C, B.T.F. Chung, Transient heat transfer in a scattering–radiating–conducting layer, J. Thermophys. Heat Transfer 13 (1999) 18–24.
[14] R. Siegel, Refractive index effects on transient cooling of a semitransparent radiating layer, J. Thermophys. Heat Transfer 9 (1995) 52–62.